Probing the Spin-Polarized Band Structure of Magnetic Weyl Semimetal $Co_3Sn_2S_2$ with Circular Dichroism in Angle-resolved Photoemission Spectroscopy

Daniel S. Shulman,[1,*] Antonio Rossi,[2,3] Vsevolod Ivanov,[2] Sudheer Sreedhar,[2] Adam L. Gross,[2] Matthew Staab,[2] Zihao Shen,[2] Eli Rotenberg,[3] Aaron Bostwick,[3] Chris Jozwiak,[3] Makoto Hashimoto,[4] Dong-Hui Lu,[4] Valentin Taufour,[2] Sergey Savrosov,[2] and Inna M. Vishik[2]

[1] *Department of Physics, University of California, Berkeley, CA 94720, USA*
[2] *Department of Physics and Astronomy, University of California, Davis, CA 95616, USA*
[3] *Advanced Light Source, Lawrence Berkeley National Lab, Berkeley, 94720, USA*
[4] *Stanford Synchrotron Radiation Lightsource, SLAC National Accelerator Laboratory, Menlo Park, CA 94025, USA*

(Dated: August 25, 2021)

Ferromagnetic ordering in the magnetic Weyl semimetal $Co_3Sn_2S_2$ occurs at $T_c = 177$ K, influencing both its topological and spin-electronic properties. Using circular dichroism in angle-resolved photoemission spectroscopy, we study the spin-polarized band structure of $Co_3Sn_2S_2$ in an attempt to observe its half-metallic nature. Though we have not yet obtained conclusive spectroscopic evidence of this half-metallicity, asymmetry in the circular dichroism appears across the Fermi level, indicating that future experiments in photoemission spectroscopy may be a promising route towards understanding the complex magnetic landscape of $Co_3Sn_2S_2$.

I. INTRODUCTION

Weyl semimetals (WSMs) are an exotic class of topological materials in which the low-energy electronic excitations form Weyl fermions [1–5]. While Weyl fermions were initially predicted in the context of particle physics in 1929 [6], so far their appearance as fundamental particles in vacuum has remained undiscovered. On the other hand, Weyl fermions have been successfully observed as quasiparticles in condensed matter, with the discovery of the first WSM compounds starting in 2015 [7–11]. Though the discovery of Weyl fermions in these initial compounds was made possible through the breaking of *inversion* ($\mathcal{I}$) symmetry, more recently, a new class of WSMs has been found in which Weyl fermions are realized through the breaking of *time-reversal* ($\mathcal{T}$) symmetry [12–14]. Because $\mathcal{T}$ symmetry is typically broken through the onset of magnetic order [15, 16], these materials have come to be known as magnetic WSMs.

One prominent magnetic WSM candidate is $Co_3Sn_2S_2$, which orders ferromagnetically at $T_c \approx 177$ K [17, 18]. The spin-resolved electronic structure of this system is of great interest due to the system's half-metallic nature [17–24]. Additionally, the formation of Weyl fermions in $Co_3Sn_2S_2$ also leads to other unusual spin phenomena such as anomalous Hall effect [25–27], chiral-anomaly induced negative longitudinal magnetoresistance [25], and giant magneto-optical response [28]. Though these studies indicate interesting magnetic features of $Co_3Sn_2S_2$, a full understanding of the magnetic landscape has yet to emerge. For instance $Co_3Sn_2S_2$ displays many complexities which are not yet understood, such as magnetic phases ranging from 90K to just below T_c [29–31], as well as magnetic domains [32] and electronic correlations [33, 34], some of which persist above T_c [35].

In this study, we use circular dichroism (CD) in angle-resolved photoemission spectroscopy (ARPES) to probe the spin-dependent band structure of $Co_3Sn_2S_2$ fig. 6. We then combine this with spin-dependent band structure calculations from density functional theory (DFT) to assess our results. This is done in order to gain a better understanding of the magnetic properties of $Co_3Sn_2S_2$, starting from the point of half-metallicity, which should have a clear spectroscopic signal. Though we observe fairly strong CD asymmetry across the Fermi level, our data also contains both positive and negative contributions to the CD signal. This is in contrast to the expectation of only one spin species across the Fermi level, leading to complications in the interpretation of our data. We thus examine some of the experimental complexities in the data, and consider the role that CD ARPES may play in future investigations aimed towards understanding the magnetic landscape of $Co_3Sn_2S_2$.

II. METHODS/TECHNICAL BACKGROUND

A. Angle-resolved Photoemission Spectroscopy

Angle-resolved photoemission spectroscopy (ARPES) is a photon-in, electron-out spectroscopy technique which is often used to probe the band structure of a material [36–40]. Standard ARPES measurements probe this band structure by obtaining a photoemission intensity $I(E, \mathbf{k})$ at each value of the binding energy E and the crystal momentum $\mathbf{k}$ of an electron from when the electron was traveling inside the solid. These quantities are related to the measured values of the experiment — the kinetic energy E_{kin} and the polar angle θ (shown in fig. 1) — through the photoelectric effect and the conservation

* svshmn@berkeley.edu

of in-plane momentum, respectively. This allows the band structure of the material to be visualized by plotting the photoemission intensity as a function of E and $\mathbf{k}$ as a color map in 2D. In these maps, higher relative photoemission intensities essentially trace out the shape of occupied energy bands, whereas lower intensities correspond to regions of ($\mathbf{k}$) space where electrons are less likely to be found.

A simplified version of the geometry for ARPES experiments is shown in fig. 1. In this setup, photons come from a controlled external light source, allowing the energy and polarization of the light to be fixed. These photons illuminate the sample at a particular spot, causing electrons from inside the material to be excited via the photoelectric effect. Photoexcited electrons escape into the vacuum according to the equation

$$E_{\text{kin}} = h\nu - \phi - |E| \tag{1}$$

with E_{kin} the kinetic energy, $h\nu$ the photon energy, ϕ the work-function of the material, and $|E|$ the binding energy of the electron. The kinetic energy is measured by the electron analyzer, which applies a voltage between two concentric hemispheres in order to select a small range of allowed kinetic energies. The analyzer is also characterized by a finite acceptance angle θ, which determines the parallel component of the crystal momentum, $\mathbf{k}_\parallel$, through the equation

$$\mathbf{p}_{\parallel,\nu} + \hbar\mathbf{k}_\parallel + \mathbf{Q} = \sqrt{2mE_{\text{kin}}}\sin\theta \tag{2}$$

This is simply a statement of in-plane momentum conservation, which arises due to translation symmetry in the x-y plane. Here, $\mathbf{p}_{\parallel,\nu}$ represents the momentum of the incoming photon, which is typically ignored due to its small contribution to the initial momentum. Note also that eq. (2) is defined only up to a reciprocal lattice vector $\mathbf{Q}$, resulting from the periodicity of momentum space in solids. In order to extract the perpendicular component of the crystal momentum, $\mathbf{k}_\perp$, some approximation is often required due to the step potential at the surface, which breaks translational symmetry along z. Nonetheless, $\mathbf{k}_\perp$ is typically a function of the photon energy, which can be varied in order to access different slices of the 3D Brillouin zone.

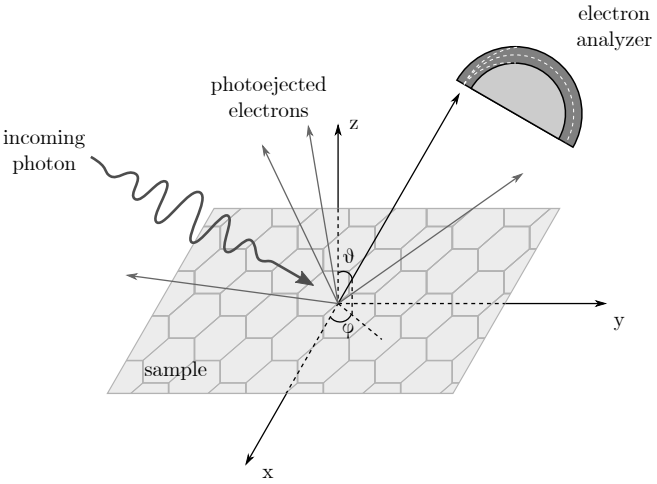

FIG. 1. Simplified schematic for the geometry of a standard ARPES experiment. Photons are shone onto the sample via an external light source, causing electrons to be photoejected in all directions. Some of these electrons are detected by the electron analyzer, which is characterized by a finite acceptance angle and kinetic energy range. The number of detected electrons is related to the photoemission intensity $I(E, \mathbf{k})$, which is then used to visualize the band structure.

B. Circular Dichroism

In CD ARPES, one takes advantage of coupling between the helicity of light and the (total) angular momentum of electrons in order to probe the spin polarization of the band structure—if certain energy bands are populated asymmetrically with regards to different spin species, then these energy bands are expected to be detectable via CD ARPES [41, 42]. Whereas standard ARPES experiments typically use linearly polarized light in order to photoexcite the electrons, CD ARPES experiments use left circularly polarized light and right polarized light, and calculate the difference between the two spectra to obtain a signal.

Here, the CD signal is defined to be the normalized difference between the ARPES intensities of spectra obtained from left circularly polarized (L) light versus right circularly polarized (R) light. That is,

$$I_{\text{CD}}(E, \mathbf{k}) = \frac{I_{\text{L}}(E, \mathbf{k}) - I_{\text{R}}(E, \mathbf{k})}{I_{\text{L}}(E, \mathbf{k}) + I_{\text{R}}(E, \mathbf{k})} \tag{3}$$

Because CD ARPES couples to the total angular momentum of electrons rather than the spin angular momentum (SAM), CD ARPES serves as an indirect probe of the spin-polarzized band structure. However, when combined with more direct techniques such as spin-resolved ARPES, CD ARPES can be used to obtain a more complete picture of the magnetic landscape. Furthermore, CD ARPES has also been successfully used to image spin polarization in a large portfolio of materials relevant to $Co_3Sn_2S_2$, such as ferromagnets [43], topological insulators [44–47] (including magnetic [48, 49] and magnetically-doped topological insulators [50]), and WSMs [51].

C. $Co_3Sn_2S_2$ structure

As shown in fig. 2, $Co_3Sn_2S_2$ crystallizes into a hexagonal shandite-type structure [24]. The corresponding Brillouin zone (BZ) contains six bulk Weyl points (three pairs), which can be found in the k_x-k_y planes lying at

$k_z = \pm 0.086 \text{Å}^{-1}$ [12]. Given that $Co_3Sn_2S_2$ is a $\mathcal{T}$-symmetry breaking WSM, this number of WPs is the minimum number allowed for this compound, due to the presence of both $\mathcal{I}$ symmetry and C_3 rotational symmetry.

The $Co_3Sn_2S_2$ structure also features an A-B-C stacking pattern along the z direction, formed by layers consisting separately of Co, Sn, and S atoms. The Co atoms form a Kagome lattice, and are responsible for the magnetic order of $Co_3Sn_2S_2$, which orders ferromagnetically at the Curie temperature $T_C = 177$ K [17, 18]. As such, the Co atoms possess a magnetic moment of $\sim 0.33\mu_B$/Co atom, which points out of plane along the c-axis. In addition, the half-metallicity of $Co_3Sn_2S_2$ is typically attributed to the Co-3d orbitals, which are the primary orbitals crossing the Fermi level in the spin-dependent band structure [18, 52].

D. Methods

To investigate the spin-polarized band structure of $Co_3Sn_2S_2$, we performed CD ARPES measurements on $Co_3Sn_2S_2$ single crystals, which were synthesized via a solution growth, as detailed in Ref. [35]. The data presented in this manuscript was collected at Beamline 5-2 of the Stanford Synchtron Radiation Lightsource (SSRL). A photon energy of 115 eV was used in order to reach the $k_z = -0.086 \text{Å}^{-1}$ slice of the Brillouin zone, which accesses the bulk Weyl points of $Co_3Sn_2S_2$ [12]. The temperature of the data is $T = 100$ K, which is below the temperature $T_c \approx 177$ K at which $Co_3Sn_2S_2$ orders ferromagnetically. Samples were cleaved in-situ at this same temperature, in an ultra-high vacuum environment with pressure no greater than 5×10^{-11} torr. The spot size of the beam has dimensions of 0.04 mm (horizontal) by 0.01 mm (vertical). While this may raise concerns relating to the mixing of surface terminations [13], we believe that these concerns have been addressed appropriately and that our data is dominated by the Sn termination, based on comparisons with previous data from Ref. [35].

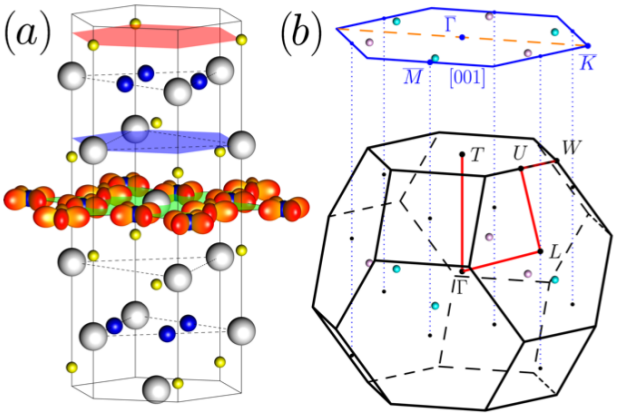

FIG. 2. Structure and BZ of $Co_3Sn_2S_2$, adapted from Ref. [35] (a) Crystal structure of $Co_3Sn_2S_2$, with Co atoms (blue), Sn atoms (white), and S atoms (yellow) shown. The red plane marks a S-type termination and the blue plane marks a Sn-type termination, while the green plane marks the Kagome lattice sub-plane. Data in this manuscript is believed to come from Sn-terminated samples. The red structures in the Kagome lattice sub-plane represent the Co-3d$_{x^2-y^2}$ orbitals, rotated in accordance with the C_3 rotational symmetry of the material. (b) BZ of $Co_3Sn_2S_2$, along with its projection along [001]. The Weyl points are shown as cyan and pink spheres, and high symmetry points are labelled appropriately. The dashed orange line in the projection indicates the $\Gamma - K$ cut used in this report.

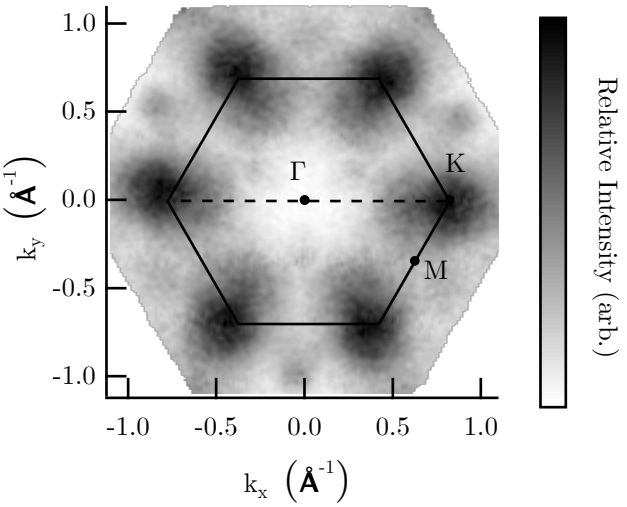

FIG. 3. FS map from standard (i.e. linearly polarized) ARPES measurements, symmetrized according to the C_3 rotational symmetry of the material. FS map is obtained using an integration window of ~ 30 meV, and the first BZ is plotted in black along with the labelled high symmetry points. The dashed black line indicates the high-symmetry cut $\Gamma - K$.

III. RESULTS

Using data from linearly polarized ARPES, we produce a Fermi surface (FS map) going through the $k_z = -0.086 \text{Å}^{-1}$ slice of the BZ, as represented by the [001] projection in fig. 2. This allows us to visualize the electronic structure of $Co_3Sn_2S_2$ near the Fermi energy, in proximity to the Weyl points of the material. The projection of the BZ along [001] at the corners is clearly visible in the FS map, which has been symmetrized according to the C_3 rotational symmetry of the material. The BZ of $Co_3Sn_2S_2$, along with labelled high symmetry points, has also been plotted on top of the FS map as shown in fig. 3. We note that though the material features C_3 symmetry, the data appear six-fold symmetric due to the ferromagnetism-induced broken $\mathbf{k} \leftrightarrow -\mathbf{k}$ symmetry along k_z, which is effectively integrated out while

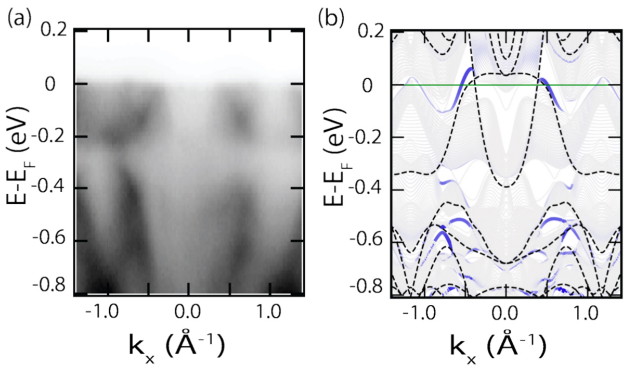

FIG. 4. High-symmetry cut $\Gamma - K$ paired with band structure calculations, adapted from Ref. [35]. (a) ARPES spectrum taken using linearly polarized light, with a temperature of 30K. (b) Slab calculations along the cut $K - \Gamma - K$. Dashed black lines indicate the bulk bands, while slab bands are colored based on their properties—blue bands indicate Sn termination surface bands, while gray bands indicate bulk bands.

producing the FS map, as explained in Ref. [35].

ARPES measurements from previous data in Ref. [35] also indicate the band structure of $Co_{3S}n_2S_2$, as shown in fig. 4. In panel a of fig. 4 we show data along the high symmetry cut $\Gamma - K$, which was taken with linearly polarized light at $T = 30$ K. Slab calculations for this cut are shown in panel b, with blue lines indicating surface bands for the relevant termination (Sn) and gray lines indicating the bulk bands. Dashed black lines are used to indicate bulk bands under standard periodic boundary conditions. Near the Fermi energy, we see that we have bands around roughly $k_x \approx \pm 0.55 \text{Å}^{-1}$, which lead to the formation of Fermi pockets near the corners of the BZ in fig. 3.

Using CD ARPES measurements, we then produce a spin polarized FS map going through the same slice of the BZ. This allows for visualization of the spin polarized features of the electronic structure, and the projection of the BZ along [001] is again clearly visible at the corners of the first BZ, as shown in fig. 5. Specifically, this is seen through the strong CD signal at the zone corners, which suggests evidence of spin polarized Fermi pockets in this region, consistent with theory. We also note that there is a strong signal in the center of the first BZ, though this corresponds to a region of low intensity based on the non spin-polarized FS map from fig. 3, suggesting that the signal in this region may be exaggerated due to normalization in eq. (3).

The spin-dependendent band structure of $Co_3Sn_2S_2$ is also visualized directly, using CD ARPES data from the high-symmetry cut along $\Gamma - K$. This data is compared to spin-dependent DFT calculations, which have been computed within the local spin density approximation (LSDA) as reported in Ref. [35].

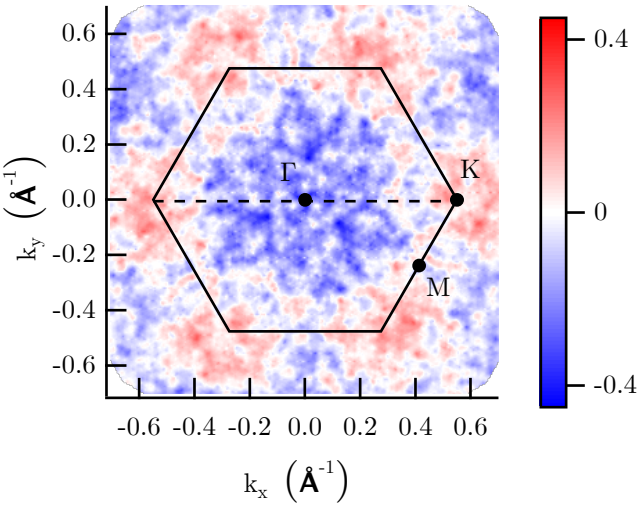

FIG. 5. FS map dichroism, symmetrized according to the C_3 rotational symmetry of the material. FS map is obtained using an integration window of 100 meV, and the first BZ is plotted in black with labelled high symmetry points and the high-symmetry cut $\Gamma - K$. The red and blue signals represent regions of uneven photoemission intensity from left and right circularly polarized light respectively, as defined in eq. (3)

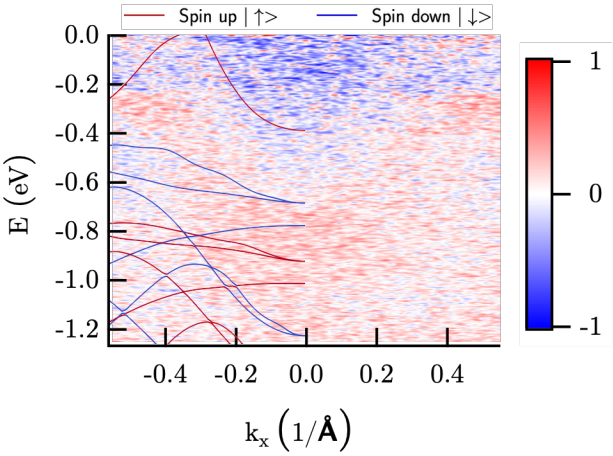

FIG. 6. CD ARPES spectrum along the high-symmetry cut $\Gamma - K$. Spin-dependent band structure calculations from DFT are overlain on the plot, and are adapted from Ref. [35]

IV. DISCUSSION

The half-metallic nature of $Co_3Sn_2S_2$ implies that there should be spin polarized bands crossing the Fermi energy. This agrees with our observations in fig. 5, in which we see a fairly strong CD asymmetry ($\sim 44\%$), which we define as the maximum value of the magnitude of eq. (3). However, the half-metallic nature of $Co_3Sn_2S_2$ also implies that bands crossing the Fermi energy should belong only to a single spin species. While we believe that the CD signal around the corners of the first BZ

(shown in red) supports the existence of spin polarized pockets for the majority species, we believe that the opposite sign signal near the center (shown in blue), which indicates the presence of the minority species, is artificially large due to the denominator in eq. (3) because of low photoemission intensities, as can be seen in fig. 3.

Furthermore, the presence of a strong CD signal near Γ may be influenced by the indirect nature of CD ARPES. The indirectness of CD ARPES, in the context of spin-resolved measurements, is most easily seen through the fact that the helicity of light couples to the total angular momentum of electrons, rather than just the spin angular momentum (SAM) [41, 42]. This suggests that contributions to the FS map can come from the orbital angular momentum (OAM) of electrons, independent of the spin-structure based half-metallic nature of $Co_3Sn_2S_2$. Previous studies performed using CD ARPES have found that OAM textures in materials can have dominant effects on the circular dichroism, even in materials already possessing strong spin splitting [44, 53].

CD ARPES is also known to be very sensitive to the experimental conditions of the experiment, such as the setup geometry and the photon energy. For instance, the setup geometry of the experiment can have an effect on not only the magnitude of the CD, but also the direction of spin polarization [41, 42]. Similarly, it has been found that the photon energy can have an effect on the sign of the dichroism, which may be flipped due to final state effects [45], suggesting that the observed CD signal may not always properly represent the intial spin polarization of electrons from when they were inside the solid. These complications can have a profound impact on the measured CD signal, leading potentially to qualitative differences in the measured FS map. Though this makes interpretation of the spin-polarized band structure more challenging, it is significant to note that the FS map produced in fig. 5 nonetheless shows spin-dependent bands crossing the Fermi level, which is an important first step towards observing half-metallicity.

More information can be obtained by looking at the cut along $\Gamma - k$ in fig. 6. One thing we note is that the CD asymmetry is much higher in the cut along $\Gamma - K$ (100%) than in the symmetrized FS map found in fig. 5 (∼44%). This supports our claim that this asymmetry is most likely artificial, and can be attributed to the fact that photoemission intensities are low (beyond observable values) at energies near the Fermi level, causing the denominator in eq. (3) to be small. This causes the CD signal to be artifically higher near the Fermi energy, affecting both the data in fig. 6 and the FS map in fig. 5.

While low photoemission intensities near the Fermi level may be attributed in part due to the quality of data, these intensities are also strongly affected by the presence of matrix element effects at these energies, which attenuate the photoemission intensity [36]. The effects of these matrix elements, which are generally a consequence of experimental details, can be seen in the linearly polarized data as well, which is not sensitive to spin polarization. For instance, in panel b of fig. 4, we compute a bulk band with parabolic dispersion centered around γ, which dips to ∼400 meV. This band is very difficult to observe however in the linearly polarized ARPES spectrum, and corresponds to the same low-energy parabolic band shown ("spin up", red) in fig. 6 from spin-dependent DFT calculations. Thus the effect of matrix elements near this band is strong, preventing a clear interpretation of the CD signal near this part of the spectrum from being made.

V. CONCLUSION

Data taken from CD ARPES indicates the presence of bands crossing the Fermi energy which are coupled to the angular momentum of electrons, though these bands contain both positive and negative contributions to the CD signal. For consistency with the half-metallic nature of $Co_3Sn_2S_2$, we expect to see a contribution from only one spin species. The region of the FS map near the center Γ in fig. 5 seems to be dominated by a negative signal (blue), but we believe that this part of the FS map is exaggerated by normalization at low intensities, and hence that this part of the signal is representative of imperfections in experiment, rather than the existence of spin polarized bands near Γ. However, there is also a portion of the FS map containing positive contributions to the signal (red) near the K points, and we believe that these contributions stem from the computed bands starting from ∼200 meV at the K points, as shown in fig. 6. Therefore, we attribute the positive signal (red) in our data to the spin majority states ("spin up") crossing the Fermi energy, and the negative signal (blue) to the spin minority states ("spin down"). Agreement with these bands however still shows room for improvement, and we note that the slab calculations in fig. 4 contain surface bands near K crossing the Fermi energy, which may be affecting the CD ARPES signal at low energies. These bands have not yet been accounted for in the spin-dependent DFT calculations however, and are beyond the scope of the present work. The data may also indicate some faint agreement along the K edge at higher energies, though further investigation is required at this point to draw further conclusions.

Future experiments may probe the spin angular momentum dependence directly using techniques such as spin-resolved ARPES, rather than doing so indirectly through CD ARPES, which is sensitive to OAM as well. However, data from CD ARPES and from spin ARPES can be compared as a way of trying to identify effects in the band structure stemming from SAM coupling and effects stemming from OAM coupling. This comparison can also be used to see how these bands are influenced by other magnetism-related complexities in $Co_3Sn_2S_2$. For instance, it is known that in-plane anomalous antiferromagnetic phases are present at temperatures as low as 90K in $Co_3Sn_2S_2$ [29], which may even affect the data presented in this report, taken at 100K. Thus,

one route for further exploration may be taking CD ARPES data at different temperatures, including ones well within the ferromagnetic regime, ones which are potentially affected by the presence of anomalous phases, and ones near T_c. The magnetization of $Co_3Sn_2S_2$ can also be controlled by doping with Ni [17, 54], which offers an alternative route towards exploring the effect of magnetism on the spin-polarized band structure without the presence of temperature-induced anomalous antiferromagnetic phases.

VI. ACKNOWLEDGEMENTS

This work was completed as part of the Research Experience for Undergraduates (REU) program at UC Davis, supported by the National Science Foundation (NSF) under grant no. 852581. D.S. would like to thank I.V. for her guidance and mentorship, as well as Rena Zieve and Nicholas Curro for their role in organizing the program. Data in figs. 5 and 6 were collected at SSRL. Use of the Stanford Synchrotron Radiation Lightsource, SLAC National Accelerator Laboratory, is supported by the U.S. Department of Energy, Office of Science, Office of Basic Energy Sciences under Contract No. DE-AC02-76SF00515. Data in fig. 4 were collected using resources of the Advanced Light Source, a U.S. DOE Office of Science User Facility under contract no. DE-AC02-05CH11231

[1] N. Armitage, E. Mele, and A. Vishwanath, Rev. Mod. Phys. **90**, 015001 (2018).
[2] S. Jia, S.-Y. Xu, and M. Z. Hasan, Nature Mater **15**, 1140 (2016).
[3] T. O. Wehling, A. M. Black-Schaffer, and A. V. Balatsky, Advances in Physics **63**, 1 (2014).
[4] B. Yan and C. Felser, Annual Review of Condensed Matter Physics **8**, 337 (2017).
[5] C. Zhang, Y. Li, D. Pei, Z. Liu, and Y. Chen, Annual Review of Materials Research **50**, 131 (2020).
[6] H. Weyl, Proc Natl Acad Sci U S A **15**, 323 (1929).
[7] S.-Y. Xu, I. Belopolski, N. Alidoust, M. Neupane, G. Bian, C. Zhang, R. Sankar, G. Chang, Z. Yuan, C.-C. Lee, S.-M. Huang, H. Zheng, J. Ma, D. S. Sanchez, B. Wang, A. Bansil, F. Chou, P. P. Shibayev, H. Lin, S. Jia, and M. Z. Hasan, Science **349**, 613 (2015).
[8] B. Lv, H. Weng, B. Fu, X. Wang, H. Miao, J. Ma, P. Richard, X. Huang, L. Zhao, G. Chen, Z. Fang, X. Dai, T. Qian, and H. Ding, Phys. Rev. X **5**, 031013 (2015).
[9] L. X. Yang, Z. K. Liu, Y. Sun, H. Peng, H. F. Yang, T. Zhang, B. Zhou, Y. Zhang, Y. F. Guo, M. Rahn, D. Prabhakaran, Z. Hussain, S.-K. Mo, C. Felser, B. Yan, and Y. L. Chen, Nature Phys **11**, 728 (2015).
[10] H. Inoue, A. Gyenis, Z. Wang, J. Li, S. W. Oh, S. Jiang, N. Ni, B. A. Bernevig, and A. Yazdani, Science **351**, 1184 (2016).
[11] R. Batabyal, N. Morali, N. Avraham, Y. Sun, M. Schmidt, C. Felser, A. Stern, B. Yan, and H. Beidenkopf, Science Advances **2**, e1600709 (2016).
[12] D. F. Liu, A. J. Liang, E. K. Liu, Q. N. Xu, Y. W. Li, C. Chen, D. Pei, W. J. Shi, S. K. Mo, P. Dudin, T. Kim, C. Cacho, G. Li, Y. Sun, L. X. Yang, Z. K. Liu, S. S. P. Parkin, C. Felser, and Y. L. Chen, Science **365**, 1282 (2019).
[13] N. Morali, R. Batabyal, P. K. Nag, E. Liu, Q. Xu, Y. Sun, B. Yan, C. Felser, N. Avraham, and H. Beidenkopf, Science **365**, 1286 (2019).
[14] I. Belopolski, K. Manna, D. S. Sanchez, G. Chang, B. Ernst, J. Yin, S. S. Zhang, T. Cochran, N. Shumiya, H. Zheng, B. Singh, G. Bian, D. Multer, M. Litskevich, X. Zhou, S.-M. Huang, B. Wang, T.-R. Chang, S.-Y. Xu, A. Bansil, C. Felser, H. Lin, and M. Z. Hasan, Science **365**, 1278 (2019).
[15] L. Balents, Physics **4** (2011).
[16] E. H. d. S. Neto, Science **365**, 10.1126/science.aax6190 (2019).
[17] T. Kubodera, H. Okabe, Y. Kamihara, and M. Matoba, Physica B: Condensed Matter Proceedings of the International Conference on Strongly Correlated Electron Systems, **378-380**, 1142 (2006).
[18] W. Schnelle, A. Leithe-Jasper, H. Rosner, F. M. Schappacher, R. Pöttgen, F. Pielnhofer, and R. Weihrich, Phys. Rev. B **88**, 144404 (2013).
[19] R. A. de Groot, F. M. Mueller, P. G. v. Engen, and K. H. J. Buschow, Phys. Rev. Lett. **50**, 2024 (1983).
[20] W. E. Pickett and J. S. Moodera, Physics Today **54**, 39 (2001).
[21] M. Holder, Y. S. Dedkov, A. Kade, H. Rosner, W. Schnelle, A. Leithe-Jasper, R. Weihrich, and S. L. Molodtsov, Phys. Rev. B **79**, 205116 (2009).
[22] L. Jiao, Q. Xu, Y. Cheon, Y. Sun, C. Felser, E. Liu, and S. Wirth, Phys. Rev. B **99**, 245158 (2019).
[23] P. Vaqueiro and G. G. Sobany, Solid State Sciences **11**, 513 (2009).
[24] R. Weihrich, I. Anusca, and M. Zabel, Zeitschrift für anorganische und allgemeine Chemie **631**, 1463 (2005).
[25] E. Liu, Y. Sun, N. Kumar, L. Muechler, A. Sun, L. Jiao, S.-Y. Yang, D. Liu, A. Liang, Q. Xu, J. Kroder, V. Süß, H. Borrmann, C. Shekhar, Z. Wang, C. Xi, W. Wang, W. Schnelle, S. Wirth, Y. Chen, S. T. B. Goennenwein, and C. Felser, Nature Phys **14**, 1125 (2018).
[26] S. Li, G. Gu, E. Liu, P. Cheng, B. Feng, Y. Li, L. Chen, and K. Wu, ACS Appl. Electron. Mater. **2**, 126 (2020).
[27] Q. Wang, Y. Xu, R. Lou, Z. Liu, M. Li, Y. Huang, D. Shen, H. Weng, S. Wang, and H. Lei, Nat Commun **9**, 3681 (2018).
[28] Y. Okamura, S. Minami, Y. Kato, Y. Fujishiro, Y. Kaneko, J. Ikeda, J. Muramoto, R. Kaneko, K. Ueda, V. Kocsis, N. Kanazawa, Y. Taguchi, T. Koretsune, K. Fujiwara, A. Tsukazaki, R. Arita, Y. Tokura, and

Y. Takahashi, Nat Commun **11**, 4619 (2020).
[29] Z. Guguchia, J. a. T. Verezhak, D. J. Gawryluk, S. S. Tsirkin, J.-X. Yin, I. Belopolski, H. Zhou, G. Simutis, S.-S. Zhang, T. A. Cochran, G. Chang, E. Pomjakushina, L. Keller, Z. Skrzeczkowska, Q. Wang, H. C. Lei, R. Khasanov, A. Amato, S. Jia, T. Neupert, H. Luetkens, and M. Z. Hasan, Nat Commun **11**, 10.1038/s41467-020-14325-w (2020).
[30] E. Lachman, R. A. Murphy, N. Maksimovic, R. Kealhofer, S. Haley, R. D. McDonald, J. R. Long, and J. G. Analytis, Nat Commun **11**, 560 (2020).
[31] M. A. Kassem, Y. Tabata, T. Waki, and H. Nakamura, Phys. Rev. B **96**, 014429 (2017).
[32] C. Lee, P. Vir, K. Manna, C. Shekhar, J. E. Moore, M. A. Kastner, C. Felser, and J. Orenstein, arXiv:2104.13381 [cond-mat] (2021).
[33] Y. Xu, J. Zhao, C. Yi, Q. Wang, Q. Yin, Y. Wang, X. Hu, L. Wang, E. Liu, G. Xu, L. Lu, A. A. Soluyanov, H. Lei, Y. Shi, J. Luo, and Z.-G. Chen, Nat Commun **11**, 10.1038/s41467-020-17234-0 (2020).
[34] R. Yang, T. Zhang, L. Zhou, Y. Dai, Z. Liao, H. Weng, and X. Qiu, Phys. Rev. Lett. **124**, 077403 (2020).
[35] A. Rossi, V. Ivanov, S. Sreedhar, A. L. Gross, Z. Shen, E. Rotenberg, A. Bostwick, C. Jozwiak, V. Taufour, S. Y. Savrasov, and I. M. Vishik, arXiv:2105.08265 [cond-mat] (2021), supplemental Information will be released upon publication, including growth details and spin-dependent DFT calculations.
[36] A. Damascelli, Phys. Scr. **2004**, 61 (2004).
[37] A. Damascelli, Z. Hussain, and Z.-X. Shen, Rev. Mod. Phys. **75**, 473 (2003).
[38] S. Hüfner, *Photoelectron Spectroscopy: Principles and Applications* (Springer Science & Business Media, 2013).
[39] D. Lu, I. M. Vishik, M. Yi, Y. Chen, R. G. Moore, and Z.-X. Shen, Annual Review of Condensed Matter Physics **3**, 129 (2012).
[40] H. Yang, A. Liang, C. Chen, C. Zhang, N. B. M. Schroeter, and Y. Chen, Nature Reviews Materials **3**, 341 (2018).
[41] W. Kuch and C. M. Schneider, Rep. Prog. Phys. **64**, 147 (2001).
[42] Y. Wang and N. Gedik, Phys. Status Solidi RRL **7**, 64 (2013).
[43] M. D. Watson, I. Marković, F. Mazzola, A. Rajan, E. A. Morales, D. M. Burn, T. Hesjedal, G. van der Laan, S. Mukherjee, T. K. Kim, C. Bigi, I. Vobornik, M. Ciomaga Hatnean, G. Balakrishnan, and P. D. C. King, Phys. Rev. B **101**, 205125 (2020).
[44] S. R. Park, J. Han, C. Kim, Y. Y. Koh, C. Kim, H. Lee, H. J. Choi, J. H. Han, K. D. Lee, N. J. Hur, M. Arita, K. Shimada, H. Namatame, and M. Taniguchi, Phys. Rev. Lett. **108**, 046805 (2012).
[45] M. R. Scholz, J. Sánchez-Barriga, J. Braun, D. Marchenko, A. Varykhalov, M. Lindroos, Y. J. Wang, H. Lin, A. Bansil, J. Minár, H. Ebert, A. Volykhov, L. V. Yashina, and O. Rader, Phys. Rev. Lett. **110**, 216801 (2013).
[46] Y. H. Wang, D. Hsieh, D. Pilon, L. Fu, D. R. Gardner, Y. S. Lee, and N. Gedik, Phys. Rev. Lett. **107**, 207602 (2011).
[47] H. Hedayat, D. Bugini, H. Yi, C. Chen, X. Zhou, G. Cerullo, C. Dallera, and E. Carpene, Sci Rep **11**, 4924 (2021).
[48] A. M. Shikin, D. A. Estyunin, I. I. Klimovskikh, S. O. Filnov, E. F. Schwier, S. Kumar, K. Miyamoto, T. Okuda, A. Kimura, K. Kuroda, K. Yaji, S. Shin, Y. Takeda, Y. Saitoh, Z. S. Aliev, N. T. Mamedov, I. R. Amiraslanov, M. B. Babanly, M. M. Otrokov, S. V. Eremeev, and E. V. Chulkov, Sci Rep **10**, 13226 (2020).
[49] C. Yan, S. Fernandez-Mulligan, R. Mei, S. H. Lee, N. Protic, R. Fukumori, B. Yan, C. Liu, Z. Mao, and S. Yang, Phys. Rev. B **104**, L041102 (2021).
[50] T. Yilmaz, G. D. Gu, E. Vescovo, K. Kaznatcheev, and B. Sinkovic, Phys. Rev. Materials **4**, 024201 (2020).
[51] M. Ünzelmann, H. Bentmann, T. Figgemeier, P. Eck, J. N. Neu, B. Geldiyev, F. Diekmann, S. Rohlf, J. Buck, M. Hoesch, M. Kalläne, K. Rossnagel, R. Thomale, T. Siegrist, G. Sangiovanni, D. D. Sante, and F. Reinert, Nat Commun **12**, 10.1038/s41467-021-23727-3 (2021).
[52] Y. S. Dedkov, M. Holder, S. L. Molodtsov, and H. Rosner, J. Phys.: Conf. Ser. **100**, 072011 (2008).
[53] V. Sunko, H. Rosner, P. Kushwaha, S. Khim, F. Mazzola, L. Bawden, O. J. Clark, J. M. Riley, D. Kasinathan, M. W. Haverkort, T. K. Kim, M. Hoesch, J. Fujii, I. Vobornik, A. P. Mackenzie, and P. D. C. King, Nature **549**, 492 (2017).
[54] I. Belopolski, T. A. Cochran, X. Liu, Z.-J. Cheng, X. P. Yang, Z. Guguchia, S. S. Tsirkin, J.-X. Yin, P. Vir, G. S. Thakur, S. S. Zhang, J. Zhang, K. Kaznatcheev, G. Cheng, G. Chang, D. Multer, N. Shumiya, M. Litskevich, E. Vescovo, T. K. Kim, C. Cacho, N. Yao, C. Felser, T. Neupert, and M. Z. Hasan, arXiv:2105.14034 [cond-mat] (2021).
[55] D. F. Liu, Q. N. Xu, E. K. Liu, J. L. Shen, C. C. Le, Y. W. Li, D. Pei, A. J. Liang, P. Dudin, T. K. Kim, C. Cacho, Y. F. Xu, Y. Sun, L. X. Yang, Z. K. Liu, C. Felser, S. S. P. Parkin, and Y. L. Chen, arXiv:2106.03229 [cond-mat] .
[56] R. Weihrich and I. Anusca, Zeitschrift für anorganische und allgemeine Chemie **632**, 1531 (2006).